Potential Performance Enhancement of a Solar Combisystem with an Intelligent Controller

Martin F. Pichler*, Hermann Schranzhofer, Andreas Heinz and Richard Heimrath

Graz University of Technology, Institute of Thermal Engineering, Inffeldgasse 25/B, 8010 Graz, Austria

Abstract: Solar thermal systems in residential buildings are generally controlled by two-level controllers, which activate solar thermal or at times with low solar radiation auxiliary energy supply into a thermal storage. Simple controllers do not have any information on actual or expected solar radiation. This leads to interference of auxiliary- and solar heat supply, which reduces the share of solar thermal energy fed into the thermal storage. Increasing accuracy of weather forecast data suggests incorporation of this information in the control algorithm. This work analyzes the maximum potential performance enhancement when applying such an intelligent predictive control. Two solar thermal systems with one auxiliary source respectively are designed in TRNSYS – these systems represent the base case. Further, a number of simulations are conducted with minor variations for the plant parameters – this gives generic results for different system configurations. In addition, each system configuration is altered to mimic the behavior of a plant with intelligent predictive control. Comparison of results indicates an improvement potential up to 10% for annual solar fractions and up to 30% for monthly solar fractions. The performance bound with respect to the annual auxiliary energy savings is approximately 8%.

Keywords: Solar thermal, predictive, weather forecast, renewable, auxiliary energy.

1. INTRODUCTION

Solar thermal (ST) systems for domestic hot water (DHW) preparation and space heating (SH) in residential buildings are generally controlled by two-level controllers. These controllers activate energy supply to a thermal storage depending on certain set- and actual-temperatures. ST energy supply happens either in the lower part of the storage, selective at different heights or *via* a stratification unit. Auxiliary heating in the upper part of the storage guarantees the compliance of set temperatures on the load side of the storage.

The inlet and outlet design for a thermal storage determines the *solar volume* (V_{solar}) and the *provision-* or *auxiliary volume* (V_{aux}), which form the total storage volume (V_S) in case of a pure bivalent system. V_{aux} may be heated by the auxiliary source or by solar energy, while V_{solar} is solely heated by solar energy, compare Figure **1**. The fact that solar energy is free and auxiliary energy costs motivates efforts to utilize solar energy as much as possible and reduce the auxiliary energy utilization. Commonly used controllers for auxiliary heating do not have any information on solar radiation or heat demand. These controllers act always according to a rigid control rule. Thus, auxiliary heating might interfere with ST heat supply reducing the share of (future) ST energy fed into the storage due to the limited storage capacity. In addition, standard controllers barely rely on a defined load schedule but rather sustain a certain temperature to assure the compliance of comfort constraints at any time.

A smart predictive control concept might be able to tackle such concurrent situations between solar and auxiliary energy input and further avoid the compliance of comfort constraints if not really needed by means of a load schedule. To decide on extended research linked to this topic, the maximum possible effect of such a controller is to be investigated.

This paper investigates the maximum theoretical auxiliary energy saving potential of an intelligent controller by means of comparing simulation results from a generic and an altered hydraulic scheme of a solar thermal system. The aim is to link different storage configurations in terms of inlets and outlets etc. to an ultimate number, which describes the performance improvement that is ideally achieved by any advanced control strategy. The maximum solar yields and minimum auxiliary heat demand and thermal storage losses obtained this way represent a performance bound for such a controller. Section 2 describes the investigated systems and provides the respective boundary conditions. Section 3 introduces the applied method and section 4 presents the results found.

1.1. Review on Measures to Reduce the Auxiliary Energy Demand

Figure **1** shows the basic scheme for a solar thermal combisystem. For residential purposes the systems are mainly designed as bivalent for which, beside the solar, a second (auxiliary) heat source feeds

*Address correspondence to this author at the Graz University of Technology, Institute of Thermal Engineering, Inffeldgasse 25/B, A-8010 Graz, Austria; Tel: +43 316 873 7312; Fax: +43 316 873 7305; E-mail: martin.pichler@tugraz.at

E-ISSN: 1929-6002/14

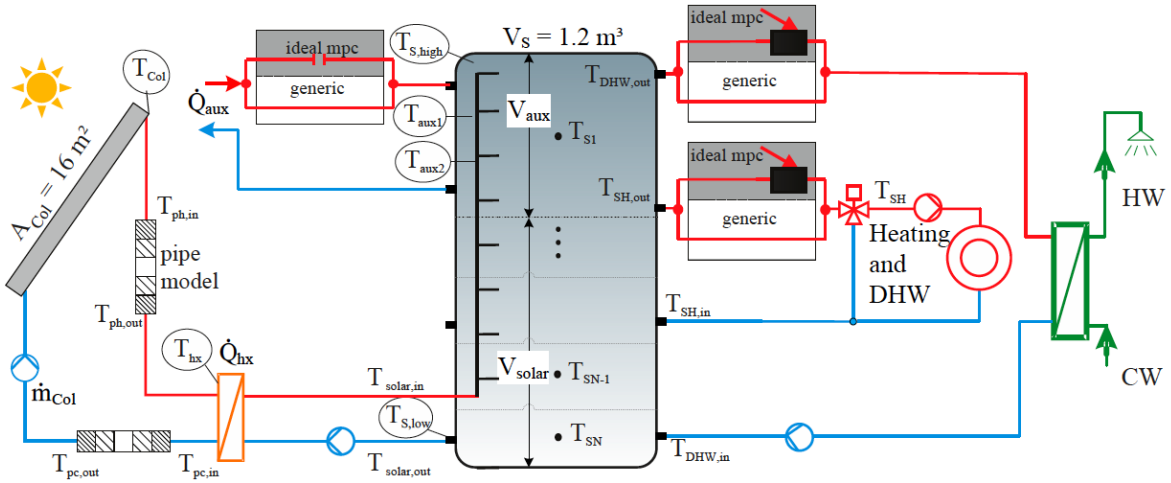

Figure 1: System hydraulics for SFH systems, principal sketch with two exclusive options for auxiliary heating.

into the thermal storage. Ideally, the whole storage is exclusively assigned to the ST system but this is impossible due to the comfort constraints. The maximization of solar energy input into the storage and the minimization of the auxiliary energy input and the storage losses have been investigated in previous research that is briefly outlined.

The optimum system configuration of a ST system in terms of storage and collector size has been analyzed extensively in [1-3]; for a concise account see [4]. The maximization of the volume V_{solar}, which is reserved exclusively for ST heat supply, is an optimization measure that generally results in higher solar fractions (F_s). However, V_{aux} cannot be eliminated, due to the relatively high power required during DHW draw-offs. Although principally possible and applied in countries of South America, it is not common in Middle Europe to install an auxiliary source with the according power to maintain the DHW draw-off due to economic reasons. Usually V_{aux} is sized such, that a daily DHW demand can be covered, i.e. 200–300 liters for a single family house (SFH); see [5].

The rule based control for charging V_{aux} depends on its actual temperature, the set temperature and the respective hysteresis thresholds of the two-level controller. This control approach requires at least one temperature sensor being placed in V_{aux}. To reduce the storage losses, the according set temperature should be as low as possible; however, a compromise between the frequency of on/off cycles of the auxiliary heating system and this temperature must be made. For efficiency measures by minimizing the storage temperatures see e.g. [6]. Haller researched and compared the one sensor approach with a two sensor approach, for which two sensors are placed in the overlap zone of V_{aux} and the SH zone of the storage at different heights [16]. The result is that this approach outperforms the one sensor approach, both concerning the number of burner starts and the auxiliary energy savings.

Depending on the solar plant operation mode (low flow or high flow), the thermal stratification in the storage is more or less important. Methods on the determination of the thermal stratification are presented in [7]. A well stratified thermal storage in connection with a stratification unit as part of the solar loop decreases the thermal losses and the auxiliary energy demand [8]. Mechanical design measures to improve the thermal stratification are dealt with in [9]. Further research on efficiency improvements for combined systems with different mechanical design has been conducted by [10, 11]. In addition to the introduced measures towards an optimal system it must be mentioned that the guarantee of ST yields comparable to simulation results and practical design in accordance with existing quality standards are still a challenge, especially for small and intermediate plants without monitoring; see [12-15].

In this work the base case is the two sensor approach, compare with Figure **1**, and it is assumed that the auxiliary source is switched on when T_{aux1} drops below 57 °C and turns off when T_{aux2} exceeds 63 °C compare with [16] or [3].

1.2. Energy Meteorology

The increasing share of weather dependent power generation and the requirement for production capacity indication on the electricity market a day ahead led to

the development of a new branch in meteorology called energy meteorology [17-19]. The frequency of forecasts increases and their accuracy is enhanced continuously with increasing importance of renewable energy (RE) generation. Various methods are used to obtain accurate forecasts for temperature, humidity, solar radiation and wind velocity. For more details see [20-23]. High quality solar radiation forecasts and further research on this, see e.g. [24], motivate the reconsideration of the control of solar thermal systems, and hold potential to boost the plant solar capacitance utilization rate (SCUR) and increase the RE yield.

1.3. Advanced Control Strategies

The first investigation on sophisticated control strategies for ST systems for residential purposes known to the authors, has been conducted at the ETH Zurich in the early eighties, see [25]. Control strategies incorporating weather forecast data showed to require less auxiliary energy than other simple strategies. On the scale of large solar thermal plants the control strategies are already elaborated and further work on the improvement of these strategies is continuously conducted [26-29]. In order to maximize the economic benefit Wittmann already proposed a complex optimization problem for scheduling the power selling at the day-ahead market [30].

With respect to small scale ST plants for residential purposes there are few research results available dealing with e.g. predictive control. An economic model predictive control (mpc) has been recently analyzed by [31], who showed through simulations that the impact of applying an economic mpc may save electricity costs up to 25-30%. Advanced pump control strategies for the solar loop are investigated in [32, 33]. However, research results on the theoretical potential for auxiliary energy savings and an increased solar yield when applying an advanced control strategy were not found.

In this research we introduce a method to determine the maximum theoretical auxiliary energy saving potential of an intelligent controller. Further, we provide results for the maximum solar yields and minimum auxiliary heat demand and thermal storage losses obtained, which represent a performance bound for such a controller.

2. DESCRIPTION OF THE SYSTEMS

This manuscript provides results for a single family house system (SFH) and for a solar thermal system being in operation in a multi-family house (MFH19).

2.1. System for a Single Family House

The object of investigation is a solar combisystem for a single family house (SFH) with a net floor area of 140 m². This SFH is considered for three different insulation standards named SFH15, SFH45 and SFH100 according to the SH energy demand approximately 15, 45 and 100 kWh/m^{2}a. Heating in SFH100 is realized by radiators (55 °C/45 °C), and for SFH15 and SFH45 by a floor heating system (35 °C/30 °C). For the simulations the Meteonorm climate data of *Strasbourg* was chosen. The building model considers occupation and internal gains resulting in a cumulated annual energy input of 9.0 and 13.4 kWh/m^{2}a. In terms of energy the DHW load profile results in 2133 kWh/a. This gives a demand of 140 L/d at 45 °C for a cold water temperature of 10 °C. In general, mass flow rates are calculated assuming a tap temperature of 45 °C, however, a weekly bathtub filling being part of the profile considers a maximum draw off temperature of 55 °C; for details see [34].

The system hydraulics in Figure **1** is used to conduct generic system simulations. With minor changes it is also used to mimic an ideally operating mpc – more on this is described in the methodology section. The aim is to maximize the ST yield, minimize the auxiliary heat demand and decrease inefficient part load operation of furnaces.

2.1.1. System Parameters and Simulation Parameters

The collector field, A_{Col} = 16 m^2, tilted by 45°, faces southwards and is operated in low flow mode with 15 kg/m^{2}h. Collector flow and return pipes (diameter 0.02 m) are 15 m each and have a coefficient of 2.5 W/(m² K) which is used to calculate the losses against the mean of current room and ambient temperature. The heat transfer coefficient (UA) of the external heat exchanger is UA = (88.561 W/(Km^2) • A_{Col} + 328.19 W/K), compare with [35]. The power of the auxiliary heater ($\dot{Q}_{aux}$) for SFH15, SFH45 and SFH100 is 2.16 kW, 4.92 kW and 8.76 kW.

Heights of storage outlets for auxiliary heating and SH and for the sensors T_{aux1} and T_{aux2} are adjusted automatically, depending on V_{aux}, V_S, and the number of nodes of the storage model (80):

$z_{rel}(T_{aux1}) = 1\text{-}0.5\ V_{aux}/V_S$, $z_{rel}(T_{aux2}) = 1\text{-}V_{aux}/V_S\text{+}2.5/80$.

The base case storage (V_S = 1.2 m^3) has an insulation thickness of 0.15 m with a conductivity of 0.04 W/mK. The effective vertical conductivity inside the storage is set λ_z = 2 W/mK. The storage losses are

calculated against an ambient temperature of 15 °C. For more details see [3]. Storage and auxiliary volume will be subject to a sensitivity analysis represented in section 4.

2.1.2. Control Settings

Solar energy supply to the storage in Figure **1** is on if T_{Col} is 5 K higher than $T_{st,low}$. Operation is sustained as long as: $T_{st,low}$< 90 °C &$T_{st,high}$< 95 °C &T_{Col}< 100 °C (stagnation). Auxiliary energy supply turns on if T_{aux1}< 57 °C and turns off if T_{aux2}> 63 °C.

2.2. System for a Multi-Family House

A ST plant (Figure **2**) for a multi-family house (MFH) with 26 flats was extensively analyzed through measurements during a national research project. The specific SH energy demand of the multi-family house is approximately 19 kWh/m^{2}a, therefore the system is abbreviated as MFH19. The solar system (A_{Col} = 34 m^2, tilted by 45° facing southwards) operating in low flow, supports the heat provision to a thermal storage of 4 m^3, from which heat is delivered to each flat for SH and DHW preparation. The measurement data enable the derivation of a realistic heat load profile incorporating both SH and DHW energy consumption. In addition validation and required adjustments of system parameters based on these measurement data allow for realistic simulation results. Although real weather data are available for the location of the plant (Wr. Neustadt) simulations presented herein were conducted using Meteonorm climate data for said location [36]. The load profile, of the thermal plant shown in Figure **2**, is derived from a building simulation with climate data of Wr. Neustadt – this leads to the SH demand. The demand for DHW purposes is obtained using measurement data from summer 2012 and extrapolation. The cumulated annual energies for the derived profile comprising DHW and the total SH demand are 56 MWh and 37 MWh, respectively. Due to unclear reasons, the histogram from the measured load return temperatures during nearly one year of time shows a clear peak at approximately 54 °C and it rarely falls below 45 °C. Since it is practically feasible to obtain return temperatures clearly below the measured data, all return temperatures were shifted by -15 K while the according power of the load was preserved. The power of auxiliary heating is limited to 120 kW. Except for the mechanical parameters, the system parameters describing physical properties and the control settings for the simulation are nearly the same as for the SFH system.

The system hydraulics in Figure **2** depicts the generic base case in terms of the storage in- and outlets. To obtain simulation results for the *ideal mpc* case a similar approach, as depicted in Figure **1** for the SFH system, was applied: The auxiliary heating into the storage is switched off, while an additional heater in the only draw-off pipe is connected in serial to cover additional energy demand in case the storage temperature does not meet the required draw off temperature.

3. METHODOLOGY

The maximum theoretical potential of an intelligent mpc is investigated by means of comparing annual

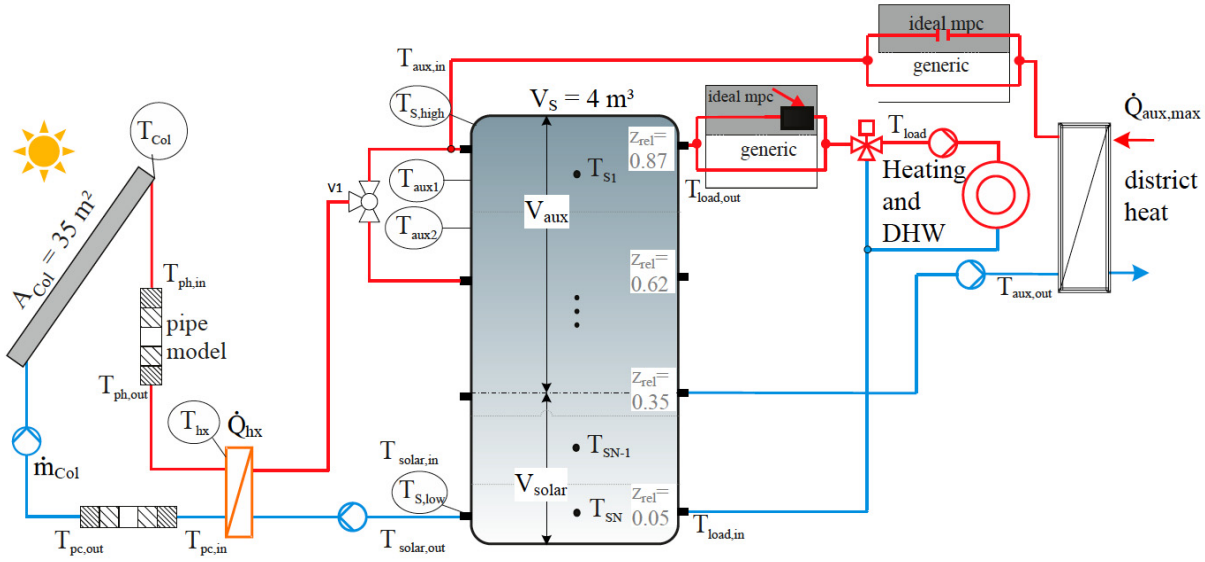

Figure 2: System hydraulics depicting the MFH19 system, *generic* configuration white part, *ideal mpc* gray part.

TRNSYS simulation results from a generic and an altered hydraulic scheme. The idea is to estimate the potential of an mpc by reserving the whole storage volume for solar energy input and compare these results with generic results. It is important to discern the two *exclusive* options for auxiliary energy provision in Figure **1**, indicated *via* three rectangular boxes each divided into two areas. The lower white area shows the relevant path for a *generic* system simulation – with auxiliary energy provision from a central auxiliary heater into the storage – and the upper gray area is relevant to obtain results for the *ideal mpc* case – with auxiliary energy provision by means of heaters outside of the storage. These heaters, being part of the supply pipe, cover any additionally required energy to provide enough heat for the building SH or for the DHW module. The described methodology applies similarly for the MFH system with only one load connected to the storage.

The according hydraulic scheme, Meteonorm weather data and the DHW and SH load profile for a SFH or a MFH form the main ingredients to obtain simulation results, see also [37]. The reliability of the simulation results depends mainly on the right choice of parameters.

Focus is given on the potential auxiliary energy savings and the change of F_s. The *base case* represents a set of usual system parameters. Any parameter variation has at least one parameter being different to the base case. The generic base case represents the generic system structure – the auxiliary heater feeds into the storage – with base case parameters. The ideal mpc base case represents the ideal mpc system structure – auxiliary heating into the storage is disconnected and auxiliary heat is supplied through a flow heater in case the required temperature is not fulfilled – simulated with base case parameters. That is any parameter variation (…_var0X) with respect to the base case parameters needs two simulations to calculate the absolute optimization potential (e.g. Delta), one for the *generic* and one for the *ideal mpc* scheme. Figure **3** shows the procedure to compare simulation results.

The shown improvement potential in terms of auxiliary energy originates from increased solar input due to extended availability of the total storage volume, and missing storage losses from the auxiliary heater feeding the storage. In a more extended mpc control concept, the mpc would also strive to operate the collector at maximum efficiency if reasonable, which is not considered herein.

3.1. Performance Indicators

Equation eq. 1 shows the calculation of the average collector efficiency (η_{col}) for a certain period – Δt is the simulation time step. Equation eq. 2 provides a measure for the system efficiency or the solar capacity utilization rate (SCUR) and eq. 3 gives the calculation for the solar fraction, where electrical devices' power consumption is not included in $\dot{Q}_{aux}$. Finally eq. 4 provides a definition characterizing the relative change of F_s for a given relative solar volume. Any of the given performance indicators may be calculated for base case parameters or a variation.

$$\eta_{Col} = \frac{1}{N}\sum_{i=1}^{N}\frac{\dot{Q}_{Col}(t_i)}{I_{gCol}(t_i)}, \quad given: \dot{Q}_{Col} \neq 0; \quad \Delta t = t_{i+1} - t_i = 2\,\text{min} \qquad \text{(eq. 1)}$$

$$SCUR = \frac{\sum_i \dot{Q}_{HXsolar}(t_i)\cdot\Delta t}{\sum_i I_{gCol}(t_i)\cdot\Delta t} \qquad \text{(eq. 2)}$$

$$F_s = \frac{\sum_i \dot{Q}_{HXsolar}(t_i)}{\sum_i \dot{Q}_{HXsolar}(t_i) + \dot{Q}_{aux}(t_i)} \qquad \text{(eq. 3)}$$

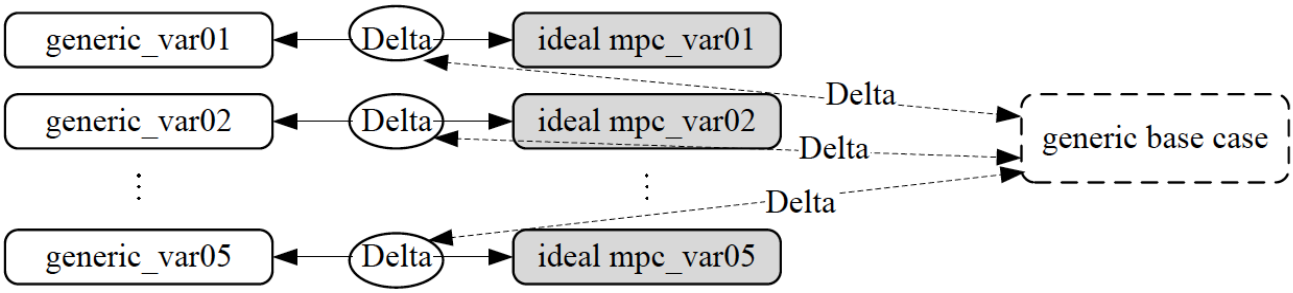

Figure 3: Simulation results-comparison procedure for parameter variations. Delta in the ellipse indicates the difference of the results when comparing the generic and the ideal mpc system structure. Delta related to the generic base case means this difference normalized with generic base case results to obtain a relative value.

$$\Delta f_s := \frac{(F_{s,ideal\,mpc} - F_{s,generic}) / F_{s,generic}}{(V_s - V_{aux}) / V_s} \quad \text{(eq. 4)}$$

4. RESULTS

Results comparing the system hydraulics *ideal mpc* and *generic* are presented for the variation of the *auxiliary volume* (V_{aux}) and the *total storage volume* (V_S); certain in- and outlet heights are adjusted accordingly.

Presented results include the F_s, the required auxiliary energy, the solar input, storage losses, and the performance indicator Δf_s characterizing the maximum relative change of F_s for a certain relative solar volume in case of applying a smart controller.

Any single results in the context of a parameter variation refer to comparison of the *generic* and *ideal mpc* case for base case parameters, which is the generic base case in Figure **3**. Results are on an annual basis if not specified otherwise.

4.1. Generic base Case Results

Table **1** provides generic base case results for the investigated systems. These results may be used to calculate relative changes of a performance indicator – indicated by the dashed lines in Figure **3**. The last column gives the required electricity energy demand (Aux. electr.). With respect to the SFH systems, half of this is consumed by the SH pump, not mentioned in the table. The *generic base case* for the MFH19 system is that, with the return pipe to the district heat heatexchanger being located at the middle storage connecting.

4.2. Variation of the Auxiliary Volume

The auxiliary volume (V_{aux}) was varied for SFH45 and MFH19 while keeping the total storage volume constant, respectively. It is expected, that the different load patterns of the SFH and the MFH systems will lead to different results and different saving potentials.

4.2.1. SFH45 System

Five values of V_{aux} between 0.1 m^3 and 0.5 m^3 were investigated for SFH45. Figure **4** shows the auxiliary energy saving potential for SFH45 when comparing *generic* and *ideal mpc* simulation results. The saving potential increases with the auxiliary volume. Especially the moderate winter months show a high saving potential. Relatively low load, high solar irradiance and limited storage capacity prevent from improvement potential in summer. The potential savings are up to 500 kWh on an annual base or approximately 9% with respect to the base case value in Table **1**.

The improvement potential in summer is quasi zero, see especially Figures **4** and **7**. The reason is relatively low load, high solar irradiance and limited storage capacity. This means that a predictive controller might improve the plant performance mainly only during spring and fall. Figure **6** shows the storage losses for ideal mpc and the generic case, reduced storage losses account for approximately one third of the reduced auxiliary energy demand.

Variation of V_{aux} for SFH45 led to the monthly and annual solar fractions shown in Figure **7**. F_s decreases slightly for the generic configuration as V_{aux} increases (white bars); this effect is marginal for *ideal mpc* – from an optimal predictive controller it is expected to compensate hydraulic schemes unfavorable for the solar yield. The annual absolute improvement potential is approximately 0.02-0.04; related to $F_{s\ base\ case}$ the increase is between 4.8% and 10.2%. March and October show an absolute improvement potential between 0.06 (14%) and 0.12 (27%). *Ideal mpc* is viable to improve F_s significantly only for relatively high V_{aux}. That is, *ideal mpc* is viable to partly compensate

Table 1: Annual Generic Base Case Results for Three SH Loads for the SFH: A_{Col}= 16 m^2, V_S = 1.2 m^3, V_{aux} = 0.3 m^3, $SFH45_{intHX}$ is with Internal Heat Exchanger; and for the Generic Base Case of the MFH19 system V_{aux} = 2.7 m^3

Base case	η_{Col} mean ± σ	$SCUR$ mean	Collector Operation[h]	F_s	DHW demand [kWh]	Heating demand [kWh]	Solar input [kWh]	Aux. input [kWh]	Storage losses [kWh]	Aux. electr. [kWh]
SFH15	0.36±0.23	0.19	1473	0.62	2132	2400	3734	2328	1547	542
SFH45	0.38±0.23	0.22	1586	0.43	2132	6476	4276	5776	1440	654
$SFH45_{intHX}$	0.36±0.22	0.20	1615	0.40	2132	6476	3989	5994	1370	657
SFH100	0.41±0.21	0.25	1689	0.27	2132	14755	4968	13284	1364	770
MFH19	0.53±0.30	0.39	1768	0.14	Total: 93139		14394	85587	6786	1061

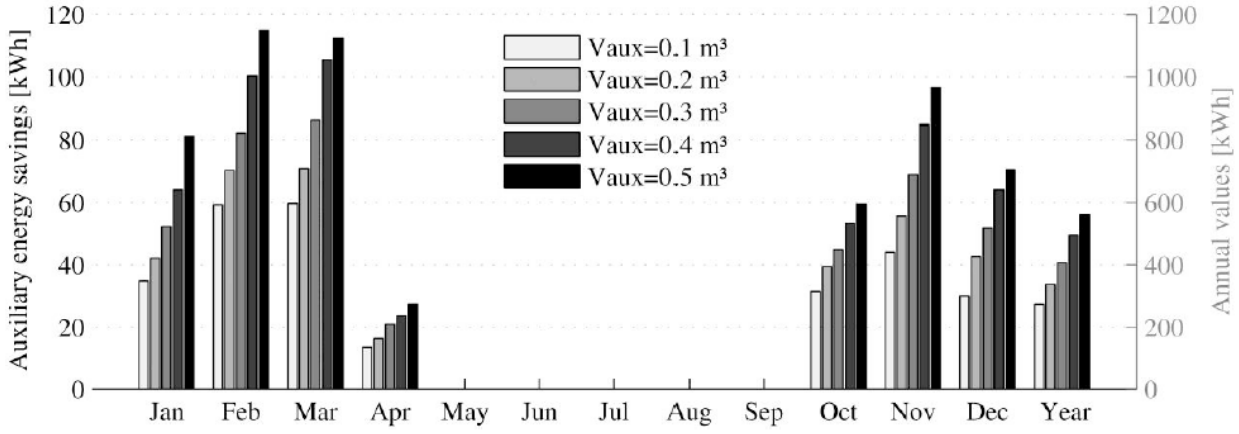

Figure 4: Auxiliary energy saving potential when comparing ideal mpc_varXX against generic_varXX results for variation of V_{aux} for SFH45 with V_S being constant 1.2 m^3; left axis relates to month, right axis to Year bars.

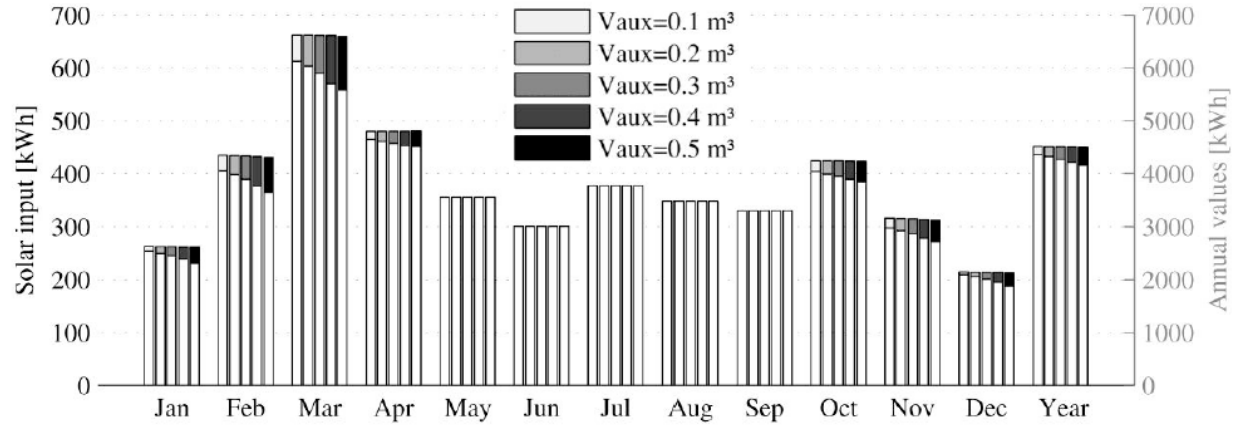

Figure 5: Solar input for the generic configuration (front: white bars) and ideal mpc (background: gray scale) for variation of V_{aux} for SFH45 with V_S being constant 1.2 m^3.

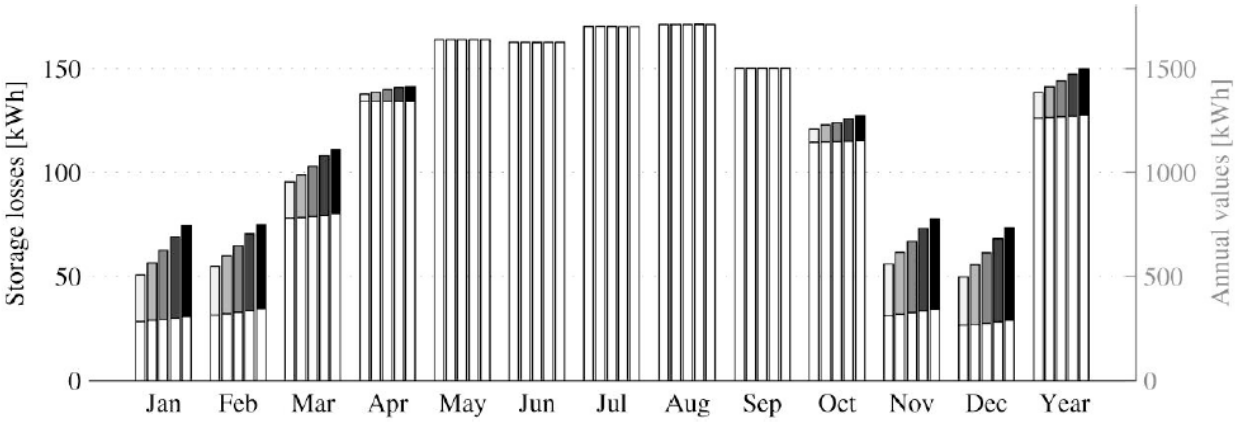

Figure 6: Storage losses for the configuration ideal mpc (front: white bars) and the generic case (background: gray scale) for variation of V_{aux} for SFH45 with V_S being constant 1.2 m^3.

the adverse effect of a lower SCUR for increased V_{aux}, which was expected. In further SFH system simulations V_{aux} = 0.3 m^3 is used to meet the required load and comfort constraints.

4.2.2. MFH19 System

Three values of V_{aux} 1.6 m^3, 2.7 m^3 and 3.8 m^3 were investigated for MFH19. Figure **8** shows the auxiliary energy saving potential when comparing *generic* and

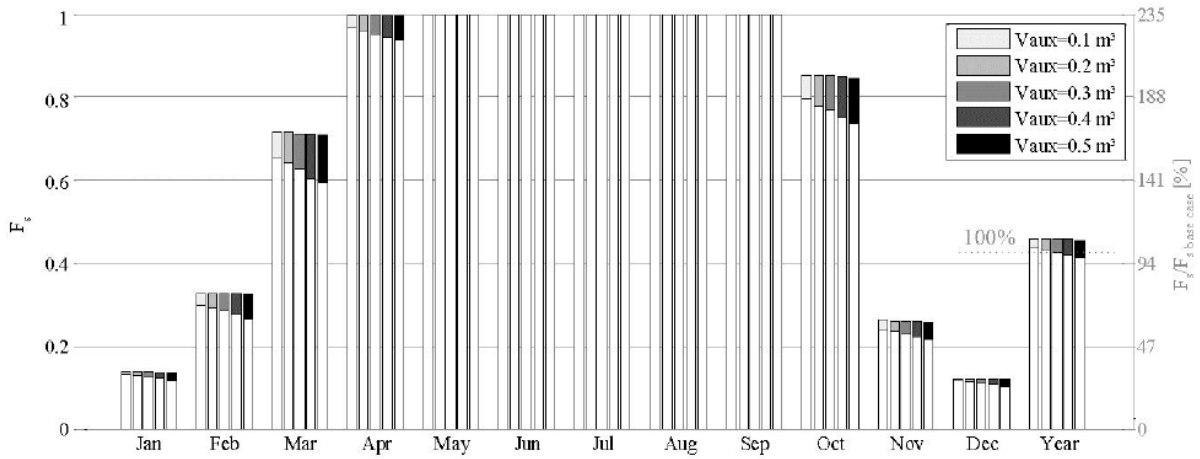

Figure 7: F_s for the generic configuration (white bars) and ideal mpc (background: gray scale bars) for variation of V_{aux} with V_S being constant 1.2 m^3 for SFH45, monthly and annual values; the right axis provides a measure related to the base case value from Table **1**.

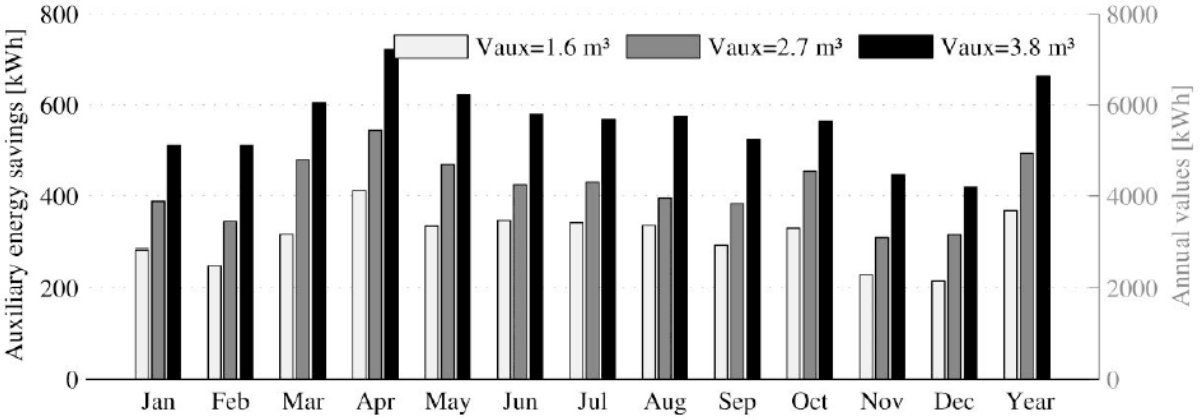

Figure 8: Auxiliary energy saving potential when comparing generic and ideal mpc simulation results for variation of V_{aux} for MFH19 with V_S being constant 4 m^3; left axis relates to months, right axis relates to the Year bars.

ideal mpc simulation results. The saving potential is significant during the whole year and increasing with the size of V_{aux}. The potential savings are up to 6600 kWh on an annual base or approximately 8% with respect to the generic base case value in Table **1**.

Figures **9** and **10** show the solar input and the storage losses for the generic configuration and *ideal mpc*, respectively. As for SFH45 an increase and a reduction of these energy fluxes are responsible for the auxiliary energy savings. The annual solar input increases up to 30% with respect to the generic base case. This effect on the solar input if applying *ideal mpc*, is much stronger compared to the results shown in Figure **5**. It can be explained by MFH19's higher SCUR – nearly twice that of the SFH45. Although the relative auxiliary energy savings are slightly less than for SFH45, comparing the two systems solar fraction (MFH19: F_S= 0.14 vs. SFH45: F_S = 0.43) allows for the conclusion that the 8% of the MFH19 are worth more than the 9% of the SFH45.

4.3. Variation of the Storage Volume

The total storage volume variation is conducted for the SFH systems only with V_{aux} = 0.3 m^3. The bar diagrams in Figures **11** and **12** show that the auxiliary energy saving potential cumulates from winter, spring and fall only and there is no additional solar input in summer for *ideal mpc*. This is due to high solar fractions of 100% in summer, compare Figure **7**. Especially a small storage volume (0.8 m^3) shows a significant potential in terms of auxiliary energy saving – 480 kWh/a or around 8% per year. The greater V_S the smaller the relative share of the auxiliary volume and the less the beneficial effect of *ideal mpc*.

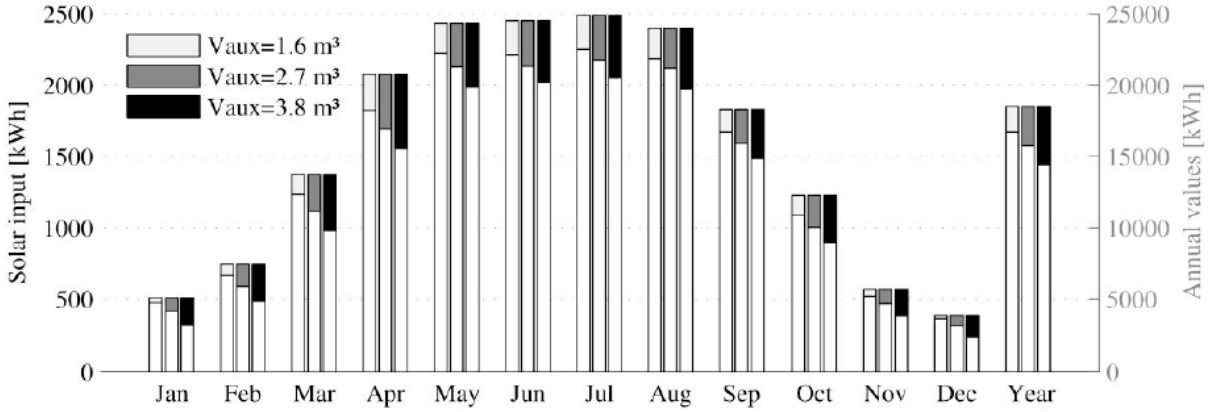

Figure 9: Solar input for the generic configuration (front: white bars) and ideal mpc (background: gray scale) for variation of V_{aux} for MFH19 with V_S being constant 4 m^3.

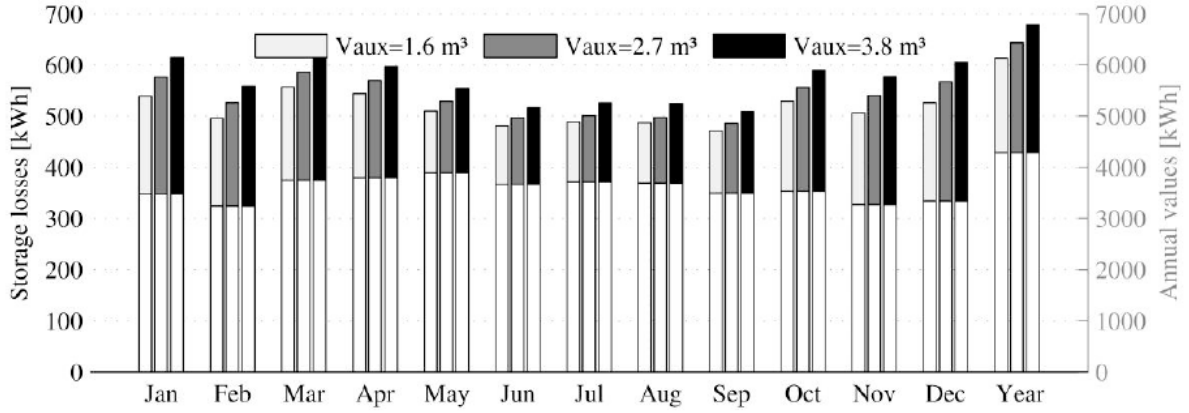

Figure 10: Storage losses ideal mpc (front: white bars) and generic case (background: gray scale) for variation of V_{aux} for MFH19 with V_S being constant 4 m^3.

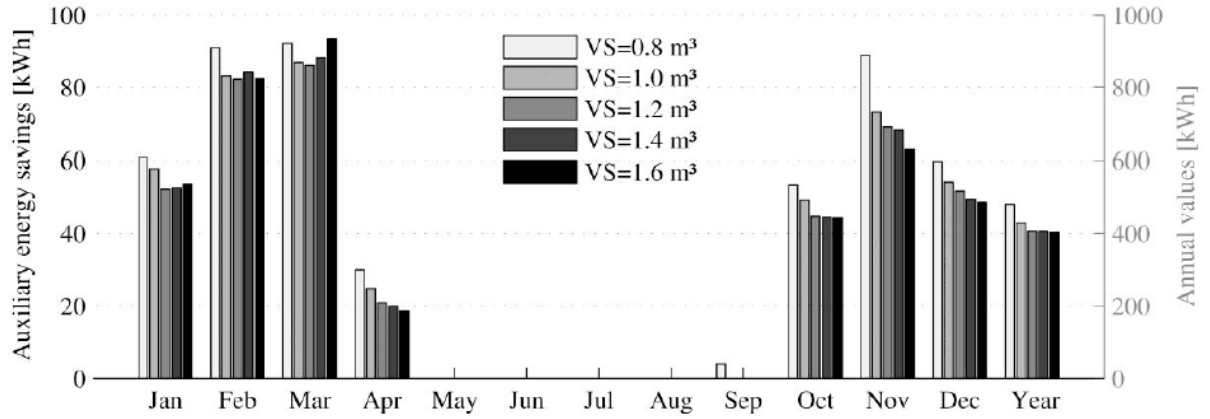

Figure 11: Auxiliary energy saving potential when comparing generic and ideal mpc simulation results for variation of V_S for SFH45 with V_{aux} being constant 0.3 m^3; left axis relates to months, right axis relates to the Year bars.

The additional solar input for *ideal mpc* decreases slightly with the storage size (Figure **12**). Cumulated differences for one year range from 308 to 210 kWh, demonstrated by the very right grayscale bars. The losses for *ideal mpc* decrease especially in the winter months similarly as for variation of V_{aux} in Figure **6**. The cumulated annual losses are approximately 12% lower for the ideal mpc case compared to the generic case. The additional solar input is a factor 1.3 greater than the difference between the storage losses, comparing *ideal mpc* and the generic case respectively.

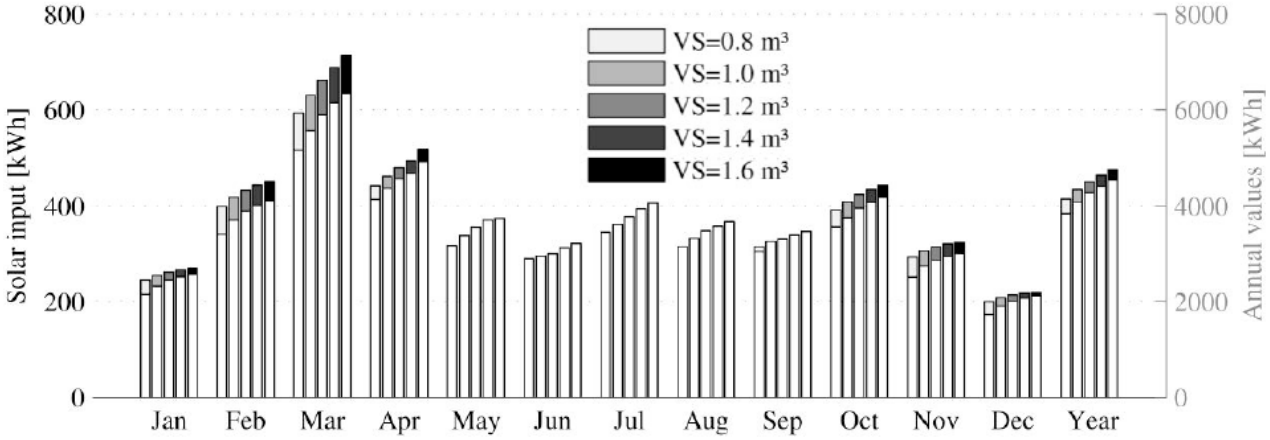

Figure 12: Solar input for the generic configuration (front: white bars) and ideal mpc (background: gray scale) for variation of V_S for SFH45 with V_{aux} being constant 0.3 m^3.

Solar fractions are drawn in Figure **13**. The annual absolute improvement potential is approximately 0.03-0.04; related to $F_{S\ base\ case}$ this gives 6.9-9.1%. March and October show a significant increase for the solar fraction, approximately 0.09 or 21%. As for the variation of V_{aux}, there is no additional improvement potential in summer.

4.4. Further Results

For the SFH system *ideal mpc* requires up to 409 kWh less auxiliary energy than the generic base case. This is mainly due to 226 kWh more solar input and 173 kWh less losses. The annual value for η_{Col} increases by approximately 1.5 percentage points (pp), and the SCUR increases by 1.2 pp for the case ideal mpc. In certain months (Feb, Nov) η_{Col} and SCUR increase by ~4 pp, or 18% with respect to the generic base case, respectively. Auxiliary heating for *ideal mpc* can be divided into operation periods lasting up to 4, 8 and 12 minutes, whereas the generic case shows only periods lasting more than 35 minutes. In praxis these short operation periods found for ideal mpc may be a problem depending on the auxiliary system, that is, a compromise between operation time an energy savings must be found. The electricity demand for the configuration *ideal mpc* increases by ~12% due to extended solar operation (~ plus 90 h for SFH45).

Simulations for SFH45 with an internal heat exchanger rather than a stratification unit show a similar picture. *Ideal mpc* requires 410 kWh less auxiliary energy (5584 kWh), the solar input increases by 211 kWh (4200 kWh) and the losses decrease by 188 kWh (1182 kWh) compared to the generic base case, respectively and on an annual basis.

Simulations for SFH100 show only a slight improvement of F_s (0.02) for variation of V_S. *Ideal mpc* requires 430 kWh less auxiliary energy than *generic*, the solar input increases by 251 kWh and the losses decrease by 180 kWh. Certain months show outstanding results in terms of auxiliary energy savings

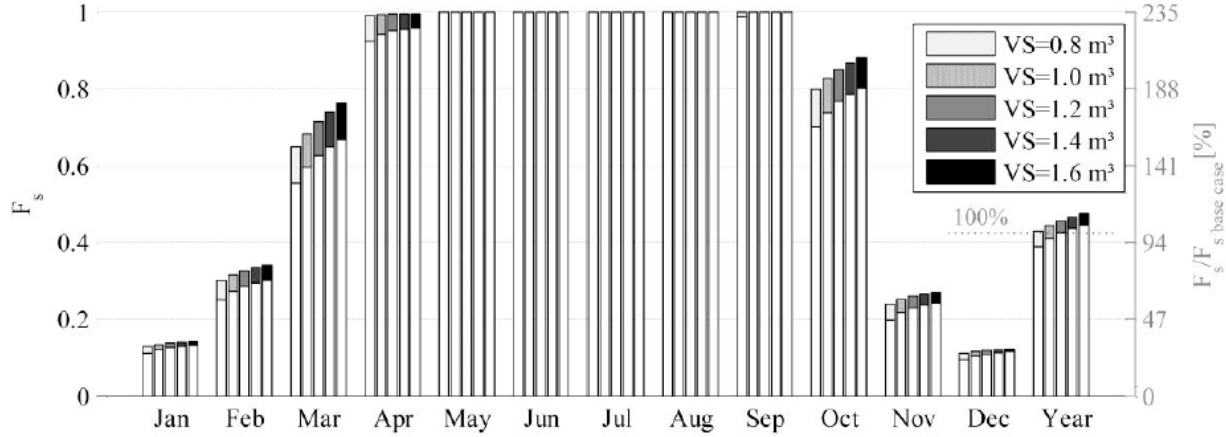

Figure 13: F_s for the generic configuration (white bars) and ideal mpc (background: gray scale bars) for variation of V_S with V_{aux} being 0.3 m^3 for SFH45; 100% relates to the base case value from Table 1.

and additional solar input with respect to the base case.

Simulations for SFH15 show the lowest absolute annual improvement potential. F_s increases by 0.03 and 0.12 (5.6% and 19.3% related to the generic base case) for *ideal mpc*, for February and March. *Ideal mpc* requires 220 kWh less auxiliary energy for the base case, the solar input increases by 186 kWh and losses decrease by 129 kWh. Auxiliary electrical consumption increases by 51 kWh.

4.5. Improvement of F_s as a Function of the Relative Solar Volume

Figure **14** shows the relative change of F_s ($\overset{def}{=} \Delta f_s$) obtained by comparing *generic* and *ideal mpc* results, as the solar volume (V_S-V_{aux}) increases. The legend elements suffixes V_s and V_{aux} indicate the conducted parameter variation for different configurations. Any results for SFH45 and SFH100 within [0.6, 0.75] relative solar volume show a decrease of Δf_s by 1 pp per 3 pp increased solar volume. Above 0.75 the system with internal heat exchanger shows a saturation indicating a higher improvement potential compared to the one with stratification unit.

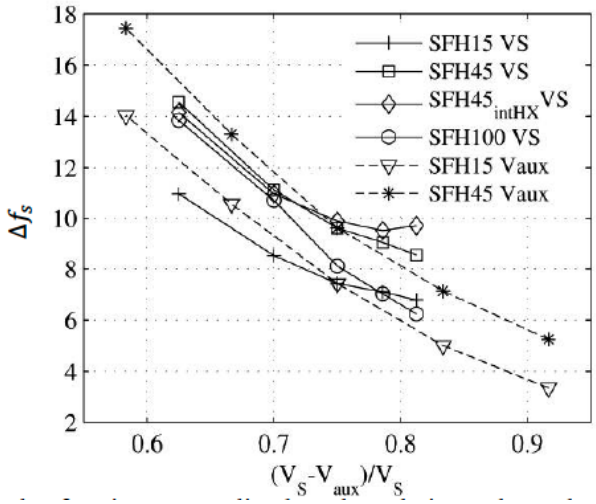

Figure 14: Change of annual solar fraction, normalized to the relative solar volume ($\overset{def}{=} \Delta f_s$), showing the relative change for ideal mpc compared to the generic case as a function of the relative solar volume. The results were obtained varying V_S or V_{aux}, except for SFH45$_{intHX}$$V_S$ solar energy input was realized with stratification unit.

A similar result as for the SFH systems is obtained for MFH19 shown in Figure **15**, although the limited number of results provides more qualitative rather than reliable quantitative information. Due to the practical restraints for this system the x-axis extends towards zero. The shape of the polygon reminds on a hockey stick. It indicates once more that especially systems with very low relative solar volume may benefit mostly from *ideal mpc*.

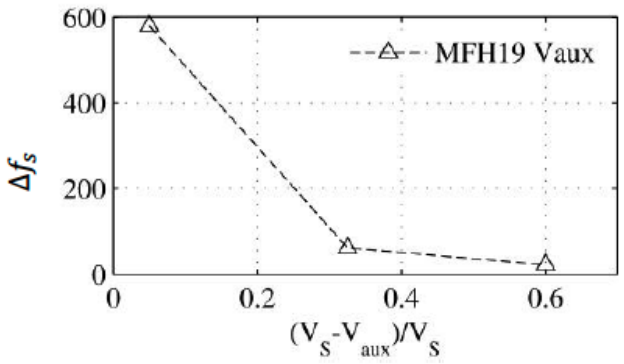

Figure 15: Compare with Figure **14** but this time for the MFH19 system.

The practical relevance of Figures **14** and **15** can be understood as follows. Given a certain relative solar volume, the expected improvement potential in percentage with respect to the generic system, when installing a predictive controller, may be calculated by the relative solar volume times Δf_s:

$$expected\ improvemt = \Delta f_s \cdot (V_s - V_{aux}) / V_s. \qquad \text{(eq. 5)}$$

5. CONCLUSION

A generic solar thermal combisystem for a SFH was designed in TRNSYS and also used to mimic an ideal weather data dependent mpc controller. Annual simulations for the ideal mpc and the generic scheme showed that the performance bound with respect to the annual auxiliary energy savings is approximately 8%. Additional simulations for a plant in a low energy MFH indicate a similar saving potential although the base case solar fraction is much lower than for the SFH system. However, the different load profile with respect to the plant size bears potential to decrease the auxiliary energy consumption also in summer, which is not the case for the SFH system. Hence, the load profile and operation conditions have a strong influence on the annual improvement potential when applying a smart controller. Approximately 5/8 auxiliary energy reduction are due to increased solar input and approximately 3/8 are due to less storage losses.

The SFH systems improvement for F_s ranges from 0.02 to 0.04, or 5% to 10% when related to the generic base case. Certain months, however, show a more significant improvement; e.g. an increase of F_s by 0.12 or 30% is possible. The average total electricity

consumption of the SFH system increases by approximately 12% for the ideal mpc scheme due to extended solar pump operation. The defined performance indicator Δf_s proved to be approximately plus 1 pp solar fraction per 3 pp increased solar volume within the interval [0.6, 0.75] for the relative solar volume. Towards a very low value Δf_s shows a hockey stick shaped characteristic indicating a high potential benefit from a smart controller for plants with low relative solar volume. Above a relative solar volume of 0.75 a saturation trend is visible.

Further research focuses on a practicable approach for an intelligent system to obtain the technically achievable performance improvement. A real application requires accurate weather forecast data and a receding horizon control algorithm. Such an approach has already been investigated and applied for heating and cooling in the building sector [39]. A model predictive approach for a smart solar tank has been recently investigated by [31].

ACKNOWLEDGEMENT

This work was conducted within the project "Prognostizierende Regelungenzur Effizienzsteigerung von Solaranlagen" (ProgReg Nr. 829826) funded by the Austrian Research Promotion Agency (FFG)

NOMENCLATURE

A_{Col} = Collector field size (m^2)

SCUR = Solar capacity utilization rate

DHW = domestic hot water

F_s = solar fractions for a certain interval (annual or monthly)

Δf_s = relative change of solar fractions for a certain relative solar volume

generic = simulation case (according results) for the standard systems

I_{gCol} = global solar radiation on the collector plane (W)

ideal mpc = simulation case (according results) for imitation of an ideal predictive controller

MFHxx = multifamily house (xx indicates the specific annual heating demand)

mpc = model predictive control

N = total number of time steps considered for summation

$\dot{Q}_{aux(\max)}$ = (maximum) power of the auxiliary heater (W)

$\dot{Q}_{Col}$ = collectorfield power (W)

$\dot{Q}_{HXsolar}$ = solar power supply at the storage (W)

SFHxx = single family house (xx indicates the specific annual heating demand)

SH = space heating

ST = solar thermal

t_i = simulation time (discrete) at the i-th step

T_{aux1}/T_{aux2} = Temperature of the sensor in the auxiliary volume at position 1/2

T_{Col} = Temperature of the sensor in a reference Collector

T_{Sj} = Temperature of the storage at the j-th node

TRNSYS = TRaNsientSYstems Simulation Program

UA = heat transfer coefficient (W/K)

V_{aux} = provision or auxiliary volume (L or m^3)

V_S = total storage volume (L or m^3)

V_{solar} = solar volume (L or m^3)

η_{Col} = collector efficiency

λ = heat conductivity (W/(mK))

REFERENCES

[1] Streicher W. Teilsolare Raumheizung – Auslegung und hydraulische Integration. Graz University of Technology 1996.

[2] Streicher W, Heimrath R. Analysis of system reports of Task 26 for sensitivity of parameters. Graz University of Technology 2003.

[3] Heimrath R, Haller M. IEA SHC-Task 32, Subtask A, The reference heating system, the template solar system. Graz University of Technology 2007.

[4] Raffenel Y, Fabrizio E, Virgone J, Blanco E, Filippi M. Integrated solar heating systems: From initial sizing procedure to dynamic simulation. Sol Energy 2009; 83: 657-63. http://dx.doi.org/10.1016/j.solener.2008.10.021

[5] Bales C, Drück H, Jaehnig D, *et al*. Solar heating systems for houses – a design handbook for solar combisystems. IEA 2003.

[6] Thür A. Compact solar combisystem–high efficiency by minimizing temperatures. Technical University of Denmark 2007.

[7] Haller MY, Cruickshank CA, Streicher W, Harrison SJ, Andersen E, Furbo S. Methods to determine stratification efficiency of thermal energy storage processes. Sol Energy 2009; 83: 1847-60. http://dx.doi.org/10.1016/j.solener.2009.06.019

[8] Glembin J, Rockendorf G. Simulation and evaluation of stratified discharging and charging devices in combined solar thermal systems. Sol Energy 2012; 86: 407-20. http://dx.doi.org/10.1016/j.solener.2011.10.013

[9] Brown N, Lai F. Enhanced thermal stratification in a liquid storage tank with a porous manifold. Sol Energy 2011; 85: 1409-17. http://dx.doi.org/10.1016/j.solener.2011.03.024

[10] Panaras G, Mathioulakis E, Belessiotis V. Investigation of the performance of a combined solar thermal heat pump hot water system. Sol Energy 2013; 93: 169-82. http://dx.doi.org/10.1016/j.solener.2013.03.027

[11] Bourke G, Bansal P. New test method for gas boosters with domestic solar water heaters. Sol Energy 2012; 86: 78-86. http://dx.doi.org/10.1016/j.solener.2011.09.004

[12] deKeizer C. Simulation-based long-term fault detection of solar thermal systems.Kassel University 2012.

[13] Krause M. Optimierungskonzept für grosse solarintegrierte Wärmeversorgungsanlagen. University Kassel 2003.

[14] Augsten E. Sonne Wind & Wärme 2012; 3: 10-1.

[15] Ullrich S. Erneuerbare Energien, Das Magazin 2013; 2.

[16] Haller Y. Combined solar and pellet heating systems – Improvement of energy efficiency by advanced heat storage techniques, hydraulics, and control. Graz University of Technology 2010.

[17] Bacher P, Madsen H, Nielsen HA. Online short-term solar power forecasting. Sol Energy 2009; 83: 1772-83. http://dx.doi.org/10.1016/j.solener.2009.05.016

[18] Fernandez-Jimenez LA, Munoz-Jimenez A, Falces A, *et al*. Short-term power forecasting system for photovoltaic plants. Renewable Energy 2012; 44: 311-7. http://dx.doi.org/10.1016/j.renene.2012.01.108

[19] Girodo M. Solarstrahlungsvorhersage auf der Basis numerischer Wettermodelle. Carl von Ossietzky Universitaet Oldenburg 2006.

[20] Perez R, Kivalov S, Schlemmer J, Hemker K Jr., Renne D, Hoff TE. Validation of short and medium term operational solar radiation forecasts in the US. Sol Energy 2010; 84: 2161-72. http://dx.doi.org/10.1016/j.solener.2010.08.014

[21] Mathiesen P, Kleissl J. Evaluation of numerical weather prediction for intra-day solar forecasting in the continental United States. Sol Energy 2011; 85: 967-77. http://dx.doi.org/10.1016/j.solener.2011.02.013

[22] Lorenz E, Remund J, Müller SC, *et al*. Benchmarking of different approaches to forecast solar irradiance. In 24th European PV Sol Energy Conf Proc 2009.

[23] Wang X, Guo P, Huang X. A review of wind power forecasting models. Energy Proc 2011; 12: 770-8. http://dx.doi.org/10.1016/j.egypro.2011.10.103

[24] Marquez R, Coimbra CF. Forecasting of global and direct solar irradiance using stochastic learning methods, ground experiments and the NWS database. Sol Energy 2013; 91: 327-36. http://dx.doi.org/10.1016/j.solener.2012.09.018

[25] Grünenfelder WJ, Tödtli J. The use of weather predictions and dynamic programming in the control of solar domestic hot water systems. In Melecon, Madrid, Spain 1985.

[26] Andrade G, Pagano D, Alvarez J, Berenguel M. A practical NMPC with robustness of stability applied to distributed solar power plants. Sol Energy 2013; 92: 106-22. http://dx.doi.org/10.1016/j.solener.2013.02.013

[27] Barigozzi G, Bonetti G, Franchini G, Perdichizzi A, Ravelli S. Thermal performance prediction of a solar hybrid gas turbine. Sol Energy 2012; 86: 2116-27. http://dx.doi.org/10.1016/j.solener.2012.04.014

[28] Camacho E, Gallego A. Optimal operation in solar trough plants: a case study. Sol Energy 2013; 95: 106-17. http://dx.doi.org/10.1016/j.solener.2013.05.029

[29] Kraas B, Schroedter-Homscheidt M, Madlener R. Economic merits of a state-of-the-art concentrating solar power forecasting system for participation in the Spanish electricity market. Sol Energy 2013; 93: 244-55. http://dx.doi.org/10.1016/j.solener.2013.04.012

[30] Wittmann M, Eck M, Pitz-Paal R, Müller-Steinhagen H. Methodology for optimized operation strategies of solar thermal power plants with integrated heat storage. Sol Energy 2011; 85: 653-9. http://dx.doi.org/10.1016/j.solener.2010.11.024

[31] Halvgaard R, Bacher P, Perers B, *et al*. Model predictive control for a smart solar tank based on weather and consumption forecasts. Energy Proc 2012; 30: 270-8. http://dx.doi.org/10.1016/j.egypro.2012.11.032

[32] Kicsiny R, Farkas I. Improved differential control for solar heating systems. Sol Energy 2012; 86: 3489-98. http://dx.doi.org/10.1016/j.solener.2012.08.003

[33] Ferhatbegovic T, Zucker G, Palensky P. Model based predictive control for a solar-thermal system. In IEEE Africon Conference Proceedings 2011.

[34] Dott R, Haller MY, Ruschenburg J, Ochs F, Bony J. The reference framework for system simulations of the IEA SHC Task 44 / HPP Annex 38 part A and part B: Buildings and space heat load. IEA 2012.

[35] Heimrath R. Simulation, Optimierung und Vergleich solarthermischer Anlagen zur Raumwärmeversorgung für Mehrfamilienhäuser. Graz University of Technology 2004.

[36] Meteonorm 7.0.21.5, Global meteorological database for engineers, planners and education, software and Data on CD-ROM; Meteotest 2013.

[37] Pichler MF, Fucak S, Frankovic B. Low temperature solar thermal domestic hot water potential of Croatia's islands and coastal regions. In Proceedings EUROSUN 2010; 2010.

[38] Hazami M, Kooli S, Naili N, Farhat A. Long-term performances prediction of an evacuated tube solar water heating system used for single-family households under typical Nord-African climate. Sol Energy 2013; 94: 283-98. http://dx.doi.org/10.1016/j.solener.2013.05.020

[39] Oldewurtel F, Parisio A, Jones CN, *et al*. Use of model predictive control and weather forecasts for energy efficient building climate control. Energy Buildings 2012; 45: 15-27. http://dx.doi.org/10.1016/j.enbuild.2011.09.022

Received on 12-05-2014 Accepted on 18-06-2014 Published on 29-08-2014

DOI: http://dx.doi.org/10.6000/1929-6002.2014.03.03.4